Aerosol flow in the Vitrocell® 24/48 exposure system: flow mixing and aerosol coalescence

Arkadiusz K. Kuczaj[a,b,*], Markus Nordlund[a], Santhosh Jarayaju[d], Ed Komen[d], Tobias Krebs[c], Manuel Peitsch[a], Julia Hoeng[a]

[a] *Philip Morris International Research & Development, Philip Morris Products S.A., Quai Jeanrenaud 5, CH-2000 Neuchâtel, Switzerland*
[b] *Multiscale Modeling & Simulation, Dept. of Applied Mathematics, University of Twente, P.O.Box 217, 7500 AE Enschede, The Netherlands*
[c] *Vitrocell Systems GmbH, Fabrik Sonntag 3, 79183 Waldkirch, Germany*
[d] *NRG, Westerduinweg 3, 1755 LE Petten, Netherlands*

Abstract

In-vitro exposure systems are increasingly used in modern toxicology assessment studies. Understanding the functioning of these complex systems and their characterization ensures well-controlled delivery of substances to cell cultures and reliable biological response of cells to the given external conditions. In this work, we present the flow mixing efficiency of the dilution unit in the Vitrocell® 24/48 (VC24/48) exposure system, together with the role of thermal coalescence. We adopted a computational fluid dynamics (CFD) approach with integrated aerosol dynamics to analyze the dilution system using high-resolution large-eddy simulations (LES). We performed simulations for three total flow rates through the system: 3 L/min, 6 L/min and 12 L/min, to investigate the influence of turbulent mixing and thermal coalescence on the aerosol characteristics. We found for all simulated flow rates that instantaneous and localized turbulent mixing is induced by the two opposing dilution jets. We found the aerosol to be uniformly mixed and the flow to be laminarized upstream of the location of the first aerosol sampling trumpet. In summary, the design of the double-tee junction, serving as the dilution unit of the VC24/48 system, guarantees efficient and localized mixing/dilution of the aerosol, whilst still delivering laminar flow towards deposition wells, when operated under these high flow-rate conditions. In addition, we showed that thermal coalescence effects do not influence the aerosol droplet size distribution during the dilution process for the studied simulation conditions.

Keywords: in-vitro, aerosol evolution, mixing, turbulent flow, coalescence, double-tee junction

List of Figures

1 Sketch of the VC24/48 exposure system functioning with the exposure module (in red) containing the double-tee dilution junction. For further details please refer to (Majeed et al., 2014) or the Vitrocell website. 5

2 Coalescence rates for three various distribution widths σ plotted in all regimes of the Knudsen number. 9

3 Time-averaged normalized velocity magnitude for 3 L/min in the (a) xz-plane, (b) xy-plane and (c-j) yz-plane at eight different diameters downstream of the mixing zone. 15

4 Time-averaged normalized velocity magnitude for 6 L/min in the (a) xz-plane, (b) xy-plane and (c-j) yz-plane at eight different diameters downstream of the mixing zone. 16

5 Time-averaged normalized velocity magnitude for 12 L/min in the (a) xz-plane, (b) xy-plane and (c-j) yz-plane at eight different diameters downstream of the mixing zone. 16

6 Iso-surfaces of the Q-criterion ($Q = +50000$) colored by normalized velocity magnitude. 17

7 Influence of dilution and droplet coalescence for initial $N = 10^{11}$ $[1/cm^3]$ and $Z = 0.02$ shown by visualization of instantaneous snapshots of the liquid mass fraction Z, droplet number density N and CMD for a developed double-tee junction mixing simulations for 3 L/min. 19

List of Tables

1 Flow parameters for the double-tee junction. 13

1. Introduction

Humans are continuously exposed to environmental or artificially produced aerosols, i.e., solid or liquid particles suspended in a gas during inhalation. These inhaled aerosols contain particles of sizes typically ranging from nano to micrometers (Hinds, 1999). Depending on the sizes and physical

*Corresponding author

Email address: arkadiusz.kuczaj@pmi.com ()

shapes of the particles, they may deposit in the airways, exposing biological tissues to substances that trigger different biological effects (Mathis et al., 2013).

To assess the toxicity of deposited aerosol constituents and their influence on biological systems, in-vivo inhalation studies are often conducted. However, when applying these standard inhalation toxicology approaches both the costs associated with the testing and the time required to conduct the assays, generate, and analyze the data makes the in-vivo approach challenging to extensively test a large number of aerosols and conditions. Furthermore, in many parts of the world there are legal, regulatory, economic, and social pressures that demand a reduction in animal testing (3R principles) and development of suitable alternatives such as in-vitro and/or in-silico testing (Schiffelers et al., 2012, European Parliament, 2010). As a result, new in-vitro/in-silico approaches need to be developed for studying the impact of aerosol exposure on potential hazards for human health.

In-vitro experimental dosimetry is increasingly used to study the effect of direct deposition on living cell cultures in exposure systems, such as air-liquid interface (ALI) systems (Thorne and Adamson, 2013, Paur et al., 2011). For example, ALI exposure systems were used by Tippe et al. (2002) to study the deposition of fine and ultrafine aerosol particles on cell cultures, whereas Comouth et al. (2013) used an ALI exposure system to study the size and the material dependent particle deposition efficiencies in the system. One particular ALI system used to systematically study the impact of cigarette smoke on the biological activity of organotypic cell cultures is the VC24/48 exposure system (Iskandar et al., 2014, Mathis et al., 2013). A similar system was also used by Neilson et al. (2015) to study the toxicity of aerosols from electronic cigarettes. The exposure in the Vitrocell system takes place in a climatic chamber in which biological tissues are placed in wells where they are exposed to the aerosol. Analytical chemistry methods are often used to analyze and quantify the deposited matter on the exposed cell cultures (Majeed et al., 2014, Adamson et al., 2014). Supplementary, biological responses (defined for various endpoints) from the tissue samples are analyzed and furthermore are integrated into systems toxicology (Hoeng et al., 2012). The ultimate goal of system toxicology research is to link biological responses from short-time tissue exposure studies with the long-term impact on biological organisms. The responses of biological organisms are not only dependent on the total applied dose of a substrate, but also on the spatial and temporal aspects of the delivery.

In-vitro exposure systems, such as the VC24/48, generally consist of delivery channels from which the aerosol flows and is sampled from. Design and construction of these systems impose mechanisms and conditions that may alter the characteristics of the flowing aerosol, affecting its deposition. Differences in the design have impact on the aerosol exposure and particle deposition, because deposition of aerosol particles is governed by the physical mechanisms, e.g., impaction, sedimentation, interception, and diffusion, which are all dependent on the flow conditions and the aerosol characteristics (Elghobashi, 1994, Guha, 1997, Hofmann, 2011). Moreover, the exposure of the tissues in in-vitro exposure systems typically involves dilution of the incoming aerosol to target a certain dosage to trigger biological effects, while still maintaining the biological tissue activity (Mathis et al., 2013).

Dilution in in-vitro exposure systems typically involves mixing the aerosol with conditioned air. The dilution may have an impact on the aerosol characteristics, i.e., its particle size, particle number density and gas-particulate phase composition, because of processes such as evaporation (droplet shrinkage), condensation (droplet growth) and coalescence (droplet clustering) (Nordlund and Kuczaj, 2015). Depending on the flow rate, particle number density, multicomponent composition and polydispersity of the investigated aerosol, the magnitudes of the above-mentioned physical processes may be altered. Moreover, the dilution air also increases the volumetric flow rate and consequently the velocity of the diluted aerosol. Depending on the particles size distribution, this increase in velocity may change the aerosol sampling efficiency (Hangal and Willeke, 1990) and particle deposition characteristics (Elghobashi, 1994, Guha, 1997, Hofmann, 2011) in the system. The mixing of the aerosol and the dilution air may also introduce non-uniformities in the particle number density and in the bulk flow. This may introduce large variability in the deposition efficiency and consequently in the dose that the tissues are exposed to. It is therefore important to understand the aerosol dynamics in the in-vitro exposure systems, and account for this when conducting exposure studies (Comouth et al., 2013). An extensive effort has been made to experimentally characterize the VC24/48 exposure system to ensure a stable and predictable delivery of cigarette smoke to the biological cell culture (Majeed et al., 2014).

As physical characterization of evolving aerosols at high particle numbers and small sizes is very challenging, computational fluid dynamics (CFD) simulations can be used to investigate and quantify the effect of the dilution on the aerosol characteristics. In this paper, we concentrate on the investigation

of the dilution and flow in a section of the VC24/48 dilution unit. In particular, we focus upon the flow-mixing efficiency and diffusion driven coalescence of droplets by studying the emerged flow patterns and uniformity of the diluted aerosol at three dilution levels. The overall intention of this study is to create awareness of the effects that the dilution system of the VC24/48 has upon the aerosol used to expose the biological tissues; the in-depth technical and mathematical details of the CFD method used are explained in the work by Nordlund and Kuczaj (2015) and Kuczaj et al. (2016). In addition, the presented material serves as a first step towards a more detailed design validation of the VC24/48 exposure system using CFD.

This paper is organized as follows: in Section 2 the VC24/48 exposure system is introduced, followed by an analysis of the aerosol dynamics in the system. Thereafter, brief overviews of the mathematical modeling approach and simulation cases are presented. The results of the simulations are presented in Section 3, followed by a general discussion of the observations in Section 4. Finally, concluding remarks are given in Section 5.

2. Materials and Methods

2.1. VC24/48 exposure system

The VC24/48 exposure system is a sophisticated and flexible platform for delivering aerosols at different concentrations and exposing them to cultured biological media. The exposure takes place in a climatic chamber, in which 48 wells with biological tissues can be exposed to the delivered aerosol simultaneously. The wells are aligned in eight rows, with six wells each for separate (parallel) or increasing (serial) aerosol dilution levels simultaneously for each row (Majeed et al., 2014). The aerosol enters the exposure system through a main aerosol delivery pipe having a diameter $D = 6$ mm. The main pipe goes back and forth over the eight rows (in Figure 1 only the schematic representation of the first row was presented together with the aerosol generator and pump unit). At the beginning of each row, two opposing dilution pipes with modifiable diameters by the so-called jet inlets (from $\oslash$0.8 to $\oslash$3 mm) are attached to the aerosol delivery pipe in a double-tee junction configuration (Figure 1). Downstream of the double-tee junction, six aerosol sampling pipes of diameters $\oslash$3 mm are connected to the main aerosol delivery pipe at a 90° angle each, sampling the aerosol from the main pipe through trumpet shaped pipes down towards the wells where the biological tissues are placed

(Figure 1). The end of each row contains a sampler towards quartz-crystal unit to monitor delivery protocol.

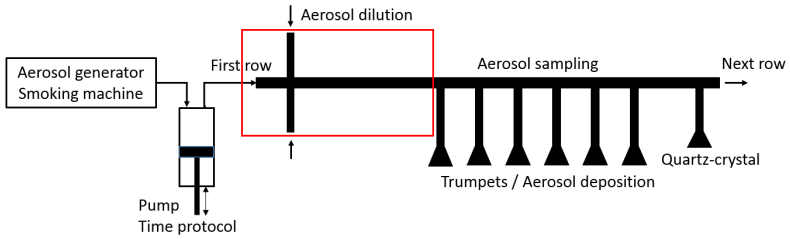


Figure 1: Sketch of the VC24/48 exposure system functioning with the exposure module (in red) containing the double-tee dilution junction. For further details please refer to (Majeed et al., 2014) or the Vitrocell website.

2.2. Aerosol dynamics in the VC24/48 exposure system

The transport, evolution and deposition of aerosol are governed by physical and chemical mechanisms. During its residence time in the VC24/48 exposure system, the aerosol travels through regions of different geometric shapes and dimensions under various flow conditions. The aerosol enters the system through the main pipe. Thereafter, the aerosol is mixed with dilution air by two opposing jets, accelerating the flow while at the same time reducing the particle number concentration during the mixing. The mixing by the two jets results in non-trivial flow dynamics in the system. According to Pan and Meng (2001), the dilution and mixing in a classical mixing tee junction with a single dilution jet can be classified by three mixing regimes, namely:

- *Jet-impaction regime*: The dilution jet is strong enough to reach the opposite wall of the pipe. Such impingement leads to a breakdown of any flow structures imposed by the main pipe flow, creating effective micro-mixing.

- *Jet-mixing regime*: The dilution jet penetrates the main flow and aligns with it, creating effective macro-mixing if the flow in the main pipe is turbulent.

- *Wall-source regime*: The dilution jet does not penetrate the main core flow deeply, but attaches to the wall, which does not support mixing.

These mixing regimes were defined for a classical mixing tee junction with a single dilution pipe. The VC24/48 exposure system has a flexible range of settings, which allows a functional set-up in all of the three regimes by modifying the inflow and dilution flow ranges, even when taking into account the two opposing jets configuration. After dilution, the aerosol is transported along the main pipe and is partially sampled at a 90° angle using a low and constant sampling flow rate. The sampled aerosol flows through the six trumpets, passes over the biological samples, where a fraction of the aerosol particles is deposited, before the rest of the aerosol is exhausted from the system. The unsampled part of the aerosol continues along the main pipe. After reaching the end of each row, the remaining aerosol travels through a smooth 180° U-turn before entering the next row where the same processes are repeated. If sequential dilution is applied, the flow rate is increased for each consecutive dilution stage with the amount of dilution air introduced. During the entire journey, the aerosol experiences a variety of conditions and may undergo dynamic evolution. Its state and how it transports, evolves and deposits in the system are dependent on the physical and chemical properties of the aerosol, the surrounding thermal and chemical environment, and the flow conditions. Because an aerosol is a gas mixture containing suspended solid or liquid particles, different physical and chemical mechanisms simultaneously govern the *transport*, *evolution*, and *deposition* of the different phases.

The main physical mechanisms governing the evolution of aerosols in the exposure system are *evaporation*, *condensation*, and *coalescence (coagulation)*, as well as gas phase *compressibility* and *dilution* (Nordlund and Kuczaj, 2015). Because the aerosol evolution mechanisms change the aerosol properties (e.g., particle size distribution and particle number density), which influence the aerosol sampling efficiency (Hangal and Willeke, 1990) and particle deposition (Hinds, 1999), it is important to be aware of their presence and implications for the exposure results. Moreover, many biological effects depend not only on aerosol particle deposition, but also on vapor uptake (Asgharian et al., 2012).

Various types of aerosols can be introduced into the exposure system, and depending on their physical and chemical characteristics, different physical mechanisms may be dominant. Respiratory aerosols are typically generated at high concentrations during the consumption of conventional and electronic cigarettes, with particle number densities of the order of $10^9 - 10^{11}$ particles per cubic centimeter (Rostami, 2009). High concentrations of aerosols are also produced for systemic delivery of therapeutic substances, because

the lungs provide a large absorptive surface area for efficient drug delivery.

In this work, we limit our exploration to low volatile aerosols with a high particle number density under stable environmental conditions, and investigate only the flow mixing efficiency of the dilution process of the VC24/48 exposure system and the influence the dilution has on the coalescence of droplets.

2.3. Modeling of aerosol dynamics

In this section, the computational framework developed by Winkelmann et al. (2015) for aerosol transport and dynamics, applicable to large numbers of species at low computational effort, is presented. Both the gas and the liquid (droplet) phases of the fluid are treated as continua and modeled in a Eulerian-Eulerian framework. The droplets are assumed to be sufficiently small, to precisely follow the flow, and to be in thermal equilibrium with the carrier phase. With these underlying assumptions, the general system of governing equations describing the transport and dynamics of a multicomponent aerosol can be expressed as (Winkelmann et al., 2015):

$$\begin{aligned}
\partial_t \rho + \partial_j(\rho u_j) &= 0 \\
\partial_t(\rho u_i) + \partial_j(\rho u_i u_j) &= -\partial_i p + \partial_j \tau_{ij} \quad ; \quad i = 1, ..., 3 \\
\rho c_p \Big(\partial_t T + u_j \partial_j T \Big) &= -\partial_j q_j - \tau_{kj} \partial_k u_j + S_h + \frac{Dp}{Dt} \\
\partial_t(\rho Y_i) + \partial_j(\rho Y_i u_j) &= -\partial_j j_{j,i} + S_i^{l \to v} \quad ; \quad i = 1, ..., n \\
\partial_t(\rho Z_i) + \partial_j(\rho Z_i u_j) &= -S_i^{l \to v} \quad ; \quad i = 1, ..., n \\
\partial_t(N) + \partial_j(N u_j) &= S_N
\end{aligned} \tag{1}$$

where ∂_t and ∂_j denote partial differentiation with respect to time t and spatial coordinate x_j respectively, and summation over j and k is implied, while no summation over i is adopted. The total mass density of the n-component system is denoted by ρ, velocity by u and temperature by T. The material derivative of the pressure is Dp/Dt, the heat capacity at constant pressure is denoted by c_p, the rate of strain tensor by τ_{ij} the dynamic gas mixture viscosity by μ, and the heat flux by q_j.

The mass fractions for the gas and liquid phases of compound i are given by Y_i and Z_i, respectively. The aerosol is assumed to behave as an ideal gas mixture, therefore connecting ρ and p through the equation-of-state.

The droplet number density N gives further information on how the liquid mass is distributed between different droplet sizes. The mass fractions are constrained by $\sum_{i=1}^{n}(Y_i + Z_i) = 1$ and droplet diffusion is neglected. The aerosol in this work is modeled by assuming a fixed log-normal droplet size distribution, described by its width σ and its count mean diameter (CMD). Transport of liquid mass fractions together with the evolving droplet number density provide information about the average aerosol droplet size in terms of the CMD. The source term related to the mass transfer between the liquid and the gas phase of species i is denoted by $S_i^{l\to v}$, whereas the source term related to the heat flow rate due to phase change is denoted by S_h. Lastly, the rate of change of the droplet number concentration $S_N = -J_c$, where J_c is the coalescence/coagulation rate. In this work, the nucleation and evaporation rates are assumed to be zero, because the focus is on mixing and coalescence effects only. The submodel for the coalescence source term is discussed next.

Coalescence modeling

Coalescence (*or coagulation*) is the process of clustering and merging of droplets because of their collisions. Coalescence is linked to the relative motion of the colliding particles, which can originate from either thermal or kinematic effects. In this work, only *thermal coalescence* is studied, even though the influence of turbulence and droplet breakup may play an important role in the close vicinity of the turbulent shear mixing region during the dilution process. *Thermal coalescence* is induced by Brownian motion existing in the carrier gas mixture in which aerosol droplets are suspended (Hinds, 1999). The chaotic movements of the gas mixture may cause neighboring droplets to collide and cause them to merge with an increasing droplet size as a consequence. In this work, it is assumed that once collided the two aerosol droplets merge, because it is unlikely that droplet bouncing will happen taking into account their small sizes and liquid nature.

Coalescence is generally dominant at high droplet number densities. As indicated by Hinds (1999), aerosol droplet number densities of the order of 10^{12} droplets per cubic meter are at the border at which coalescence effects start to play a role. Although dilution in the VC24/48 exposure system generally decreases the droplet number density, the particular mixing setup with collapsing jets in the dilution unit may cause locally increased droplet number densities, because of the narrowing of the aerosol flow paths. The amount of coalescence occurring does not only depend on the droplet number density,

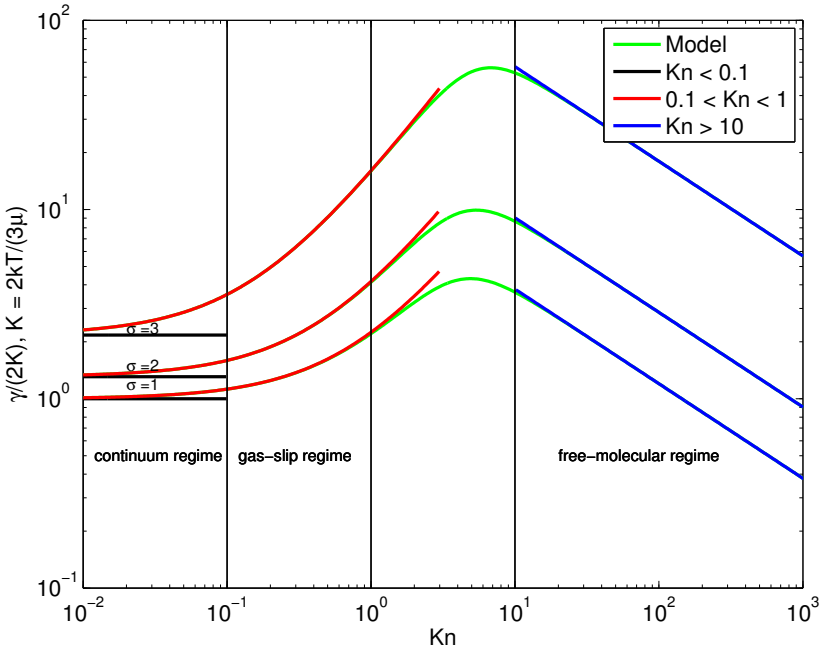


Figure 2: Coalescence rates for three various distribution widths σ plotted in all regimes of the Knudsen number.

but also on the droplet size distribution, because droplets of various sizes may collide with each other. Lee and Chen (1984) proposed a coalescence model for polydisperse aerosols that is reduced to $J_c = \gamma\ N^2$, where γ is the coalescence rate coefficient, for log-normal distributions (Lee and Chen, 1984).

The intensity of Brownian motions is dictated by the Knudsen number, $\mathrm{Kn} = 2\lambda\ /\mathrm{CMD}$, where λ is the mean free path of the carrier gas mixture. The Lee and Chen model is valid for the free-molecular regime $\mathrm{Kn} > 10$ and for the gas slip regime $\mathrm{Kn} < 1$. These two regimes are asymptotically aligned with a continuum regime, where the coalescence rate is dictated by the Smoluchowski constant $K = \frac{2kT}{3\mu}$, where k is the Boltzmann constant and μ the dynamic gas mixture viscosity. Coalescence rate γ within $1 < \mathrm{Kn} < 10$ is unknown as indicated by Lee and Chen (1984). To computationally model all regimes, coalescence rate γ needs to be approximated between the known regimes as shown in Figure 2 for various distribution widths σ. The two

known regimes are for Kn < 1:

$$\gamma_l = \frac{2kT}{3\mu}\Big(1 + \exp(\ln^2(\sigma)) + \frac{2.49\lambda}{d_m}\Big[\exp(2\ln^2(\sigma)) + \exp(4\ln^2(\sigma))\Big]\Big)$$

and Kn > 10:

$$\gamma_s = \sqrt{\frac{3kTd_m}{\rho_l}}\Big(1 + \frac{1}{\sigma}\Big)^{-1/2}\Big[\exp\Big(\frac{19}{8}\ln^2(\sigma)\Big) + 2\exp\Big(-\frac{1}{8}\ln^2(\sigma)\Big) + \exp\Big(-\frac{5}{8}\ln^2(\sigma)\Big)\Big]$$

while between them:

$$\gamma = \Big(\gamma_l^{-2} + \gamma_s^{-2}\Big)^{-1/2}$$

The conversion from the diameter of average mass d_m to CMD follows the Hatch-Choate conversion equation for log-normal distributions (Hinds, 1999), i.e.:

$$\text{CMD} = d_m \exp(-\frac{3}{2}\ln^2(\sigma))$$

A direct application of the coalescence source term $J_c = \gamma\ N^2$ will not necessarily preserve positivity of the particle number density N solution. Therefore, the coalescence term is integrated over the computational time step to ensure particle number density positivity and entered into the equation (1).

Turbulence modeling

Turbulence (often characterized by the Reynolds number) originates from small-scale perturbations, which depending on their intensity, introduces velocity fluctuations leading to irregular and chaotic behavior of the flow (Pope, 2000, Tsinober, 2009). In the dilution unit of the VC24/48 exposure system, turbulent mixing is expected where the aerosol and two dilution flow jets meet in the double-tee junction of the main pipe. Hence, capture of this turbulent mixing behavior is required for accurate prediction of the flow and its effect on the mixing and aerosol characteristics. To capture turbulent effects when solving the discretized system of equations, the spatial resolution of the computational mesh must fulfill certain requirements dictated by the typical magnitude (size) of those fluctuations. For industrial applications, the direct numerical simulation (DNS) approach where the complete

spectrum of physical scales is resolved is often not feasible, even for moderate turbulent flows, because of the computational cost. In the large-eddy simulation (LES) approach, the large three dimensional eddies created in the flow due to the geometry and boundary conditions are directly resolved, whereas the small more isotropic eddies are modeled using a subgrid-scale model (Geurts, 2003). Despite being computationally intensive, LES is seen as a reliable, advanced turbulence modeling alternative to the costly DNS or inaccurate Reynolds averaged Navier-Stokes (RANS) approach often used for industrial applications (Deissler, 1998).

The considered double-tee mixing flows are characterized by the low Reynolds numbers (see Section 2.4) and one can fairly resolve important flow features applying proper mesh guidelines for the geometry discretization (Kuczaj et al., 2010), and performing quasi direct numerical simulations (quasi-DNS) (Komen et al., 2014). Accordingly, we adopt both high-resolution methods, i.e., LES technique (using a subgrid-scale model introduced by Vreman (2004)), and DNS method (as presented with equations (1) and computational results in Section 3). More details concerning the assumptions, validation and the implementation of the DNS and LES approaches can be found in Kuczaj et al. (2016).

Numerical method

The governing equations and the related submodels are implemented into the extended pressure implicit with splitting of operator (PISO) algorithm for aerosol dynamics developed by Frederix et al. (2015) using the OpenFOAM® open source software package version 2.3.0. The segregated, collocated variable finite-volume algorithm based on the original PISO approach by Issa et al. (1991) is used for solving the equations of fluid motion.

2.4. Case descriptions

In this section, the computational geometry, mesh and simulation conditions presented were used for the investigations of the flow and mixing in the dilution unit, followed by a study of potential coalescence effects resulting from the dilution.

Geometry

The geometry adopted for the investigations of the mixing and coalescence effects in the dilution unit was constructed as a double-tee junction that spans in length from the aerosol inlet up to the first aerosol sampling point,

i.e., the first trumpet pipe. The computational domain for such a double-tee junction, represents the dilution part of a single row of the exposure system shown in Figure 1. This reduced geometry was chosen to diminish the computational cost for the considered cases and to allow for high resolution simulations. The dimensions of the computational domain are based on the VC24/48 exposure system. The main pipe has a diameter $D = 6$ mm and the diameters of the two dilution pipes are $D/2$. The main pipe extends 8.3 diameters upstream of the double-tee junction and 30 diameters downstream. The length of each dilution pipe is 6.3 diameters.

Computational mesh

The computational mesh was generated using polyhedral elements. The mesh close to the double-tee junction was created using polyhedral elements with wall boundary layers. The generated mesh was then extruded in the axial direction on both sides of the tee junction. Special care was taken to generate computational mesh with high enough resolution to accurately capture the flow and mixing phenomena for the highest flow rate simulated. Following work by Kuczaj et al. (2010) for the meshing of a single-tee junction, the mesh for the double-tee junction was based on non-dimensional cell sizes calculated for the highest flow rate simulated, i.e., 12 L/min in the main pipe. The total mesh size was about 2.6 million cells. The same mesh was also used for the simulations of lower flow rates for consistency reasons. Results obtained by Komen et al. (2014), Kuczaj et al. (2016) demonstrated that the flow results obtained using such an approach are mesh-independent.

Simulation conditions

Three computational cases were considered for the double-tee junction flow simulations, with flow rates representative of the typical working range of the VC24/48 dilution capacity. For the three cases, the total volumetric flow rates downstream of the double-tee junction were 3, 6 and 12 L/min. The system usually operates up to 4 L/min according to Adamson et al. (2014), but flow rates up to 12 L/min were reported by Thorne and Adamson (2013). The higher flow rates in this work were chosen to explore the upper limit of mixing in the exposure system. The flow rate in each of the two dilution pipes was half that of the main pipe prior to reaching the double-tee junction. The flow rates, together with their associated bulk Reynolds number, $Re = \frac{\rho U D}{\mu}$, where U is the bulk velocity downstream of the mixing zone, are summarized in Table 1 for the three considered cases.

Table 1: Flow parameters for the double-tee junction.

Case	Main inlet flow rate (L/min)	Dilution inlet flow rate (L/min)	Total flow rate (L/min)	Bulk Reynolds number
1	1.5	0.75	3	636
2	3	1.5	6	1271
3	6	3	12	2542

For the simulations concerning flow and mixing, the computational domain was initialized with zero velocity, a temperature of 37°C, and atmospheric pressure; simulations were performed with air as the working fluid. The desired constant flow rates with inlet temperatures of 37°C were applied at the main inlet and at the two dilution inlets. No turbulent fluctuations were applied at the domain inlets. Atmospheric pressure was applied at the domain outlet and zero pressure gradient boundary conditions were applied at the three domain inlets. Parabolic velocity profiles were applied to all inlets, because the Reynolds number indicates that the incoming flow is laminar. In real exposure studies, the aerosol is introduced into the system following specific flow protocols that incorporate puffing, presumably with sinusoidal or square puff-profile, followed by a break in the aerosol inflow, while maintaining continuous air dilution flow through the system (Majeed et al., 2014, Neilson et al., 2015). Such sequential dilution of the aerosol may lead to additional variations of the aerosol characteristics, being out of scope for the present investigation.

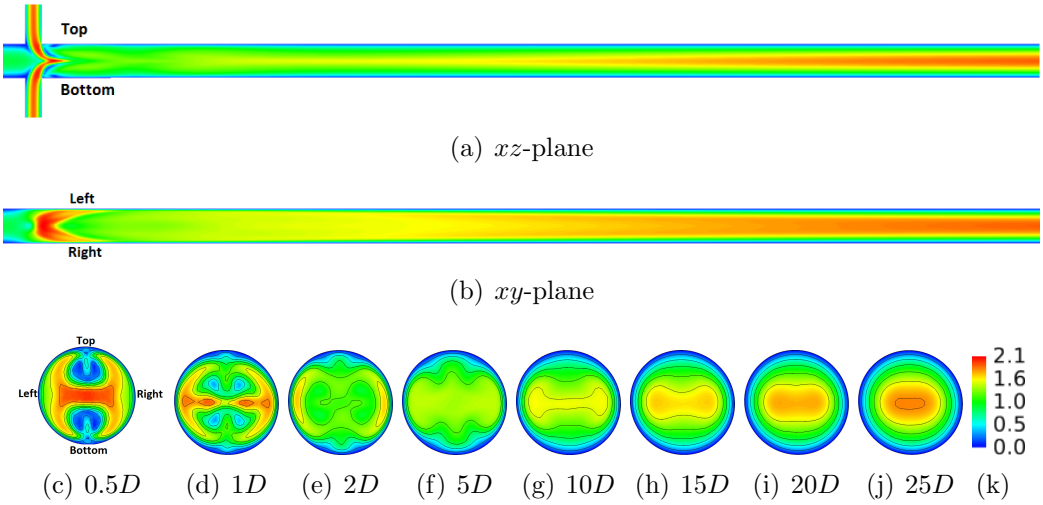
For studying coalescence effects, identical geometry, mesh and conditions were used as for the flow simulations. The volumetric flow rate was 3 L/min. The temperature, pressure and velocity conditions were identical to that of the flow simulation having the same flow rate. In contrast to the flow simulations, an aerosol consisting of liquid droplets of density 1000 kg/m^3 suspended in air was prescribed at the inlet of the main pipe. The droplet size distribution was assumed to be log-normal with a width of $\sigma = 4/3$. Under this prescribed log-normal distribution, the aerosol droplet size can be calculated from the total liquid mass fraction and the droplet number density (Hinds, 1999). The CMD of the aerosol considered in this work was chosen to be $0.7 \cdot 10^{-6}$ m, which is a typical size for respirable aerosols; with a droplet number density of $N = 10^{11}$ cm^{-3}. The liquid mass fraction, Z, prescribed at

the inlet boundary of the main pipe was taken from the relationship between CMD and N. The considered high particle number density (N) for the typical aerosol droplet size of interest (CMD) is introduced to study the most severe conditions for the coalescence that can be present in the system. This would require that the generated aerosol smoke is directly injected into the dilution unit in the first row. The experimental time protocol as sketched in Figure 1 causes long residence time for the aerosol either in the pump (first row) or caused by the flow delay (consecutive rows). From this perspective, the studied case is conservative for all other conditions at lower particle number densities reported in the literature.

3. Results

3.1. Flow mixing simulations

The time-averaged normalized velocity magnitudes for the three considered flow rates are shown in Figures 3-5 for different coordinate planes. For all flow rates, the volumetric flow rate in each of the dilution inlets was half of that of the main inlet. Given that the diameters of the dilution inlets were half of the main inlet, the velocities in each of the dilution inlets were twice that of the main inlet. The time-averaged normalized velocity magnitude is derived from the numerical solution as $\sqrt{u^2 + v^2 + w^2}/U$; where u, v and w are the three time-averaged mean velocity components (u_i). The bulk velocities downstream of the mixing zone were $U = 1.768$, $U = 3.537$, and $U = 7.074$ m/s for three flow rates. For all three flow rates, the high velocity jets coming from the top and bottom dilution pipes interacted with the flow coming from the left through the main pipe inlet. These jets turn in the axial direction at the double-tee junction (Figures 3a, 4a, 5a), creating an extensive and wide shear layer in the middle of the junction. At these substantial flow rates, the mixing in the double-tee junction can therefore be considered to be in the *jet-mixing regime* for all three flow rates; this regime is known to create effective macro-mixing when the flow is turbulent. A little further downstream of the double-tee junction, the two velocity jets from dilution pipes were merged together, forming a high velocity cone-like structure at the center of the main pipe. Because of the acceleration at the center, two recirculation zones were formed on the top and bottom side of the visible cone shear-flow structure. These recirculating, secondary flow zones were most pronounced for the 3 L/min flow rate. The aerosol flow coming from the main pipe tended to circumvent the velocity jets from the two opposing



(a) xz-plane

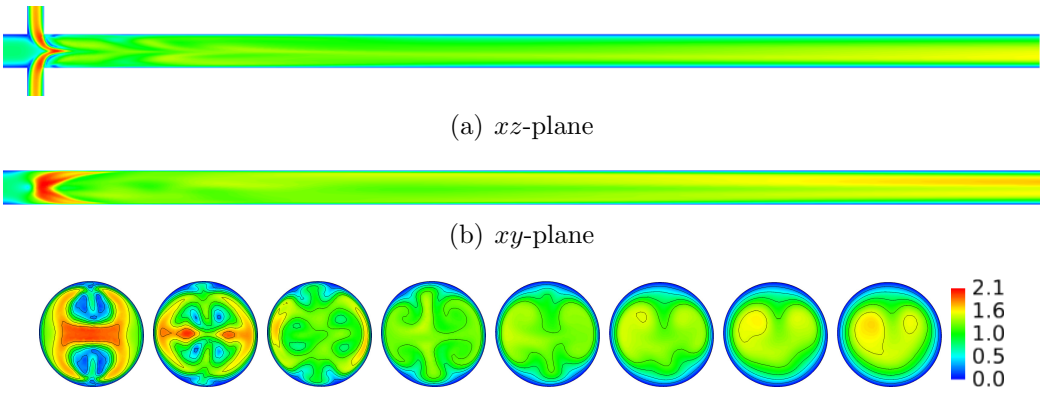
(b) xy-plane

(c) $0.5D$ (d) $1D$ (e) $2D$ (f) $5D$ (g) $10D$ (h) $15D$ (i) $20D$ (j) $25D$ (k)

Figure 3: Time-averaged normalized velocity magnitude for 3 L/min in the (a) xz-plane, (b) xy-plane and (c-j) yz-plane at eight different diameters downstream of the mixing zone.

dilution pipes. This can be seen in the normalized velocity in the xy-plane that is increased around the incoming dilution jets shown in Figures 3b, 4b, 5b for the three flow rates. This can also clearly be seen in Figures 3[c-d], 4[c-d], 5[c-d].

Further downstream, the three flow rates demonstrated different flow characteristics. For 3 L/min, the normalized velocity profiles show symmetry properties, both in the xz-plane (cf. Figure 3a) and in the xy-plane (cf. Figure 3b). For this flow rate, the velocity profile tended to laminarize and develop into a parabolic/fully-developed profile prior to the outlet, representing the location of the first aerosol sampling trumpet in the VC24/48 exposure system. For higher flow rates, the velocity profiles demonstrated more asymmetric behavior, forming streaks of high and low velocities. For both the 3 L/min and the 6 L/min flow rates, the flow eventually laminarized reaching the outlet (Figures 3[e-j] and 4[e-j]), whereas it was not the case for the 12 L/min flow rate (Figures 5[e-j]). This is further visualized in Figure 6, which shows the iso-surfaces extracted for a very high positive value of the so-called Q-criterion (i.e., +50000), which represents regions of highly rotational flow (Hunt et al., 1988, Dubief and Delcayre, 2000). For the 3 L/min flow rate, highly rotational flow was observed in the first few diameters downstream of the double-tee junction. For 6 and 12 L/min, the rota-

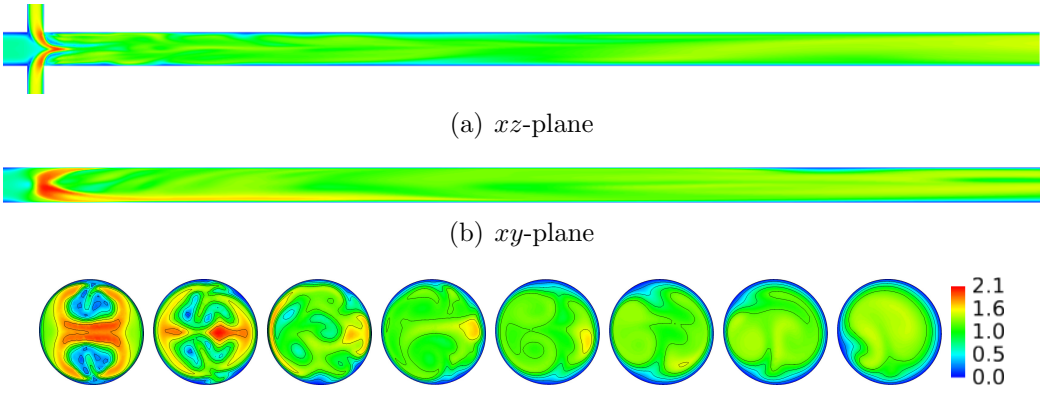


(a) xz-plane

(b) xy-plane

(c) $0.5D$ (d) $1D$ (e) $2D$ (f) $5D$ (g) $10D$ (h) $15D$ (i) $20D$ (j) $25D$ (k)

Figure 4: Time-averaged normalized velocity magnitude for 6 L/min in the (a) xz-plane, (b) xy-plane and (c-j) yz-plane at eight different diameters downstream of the mixing zone.

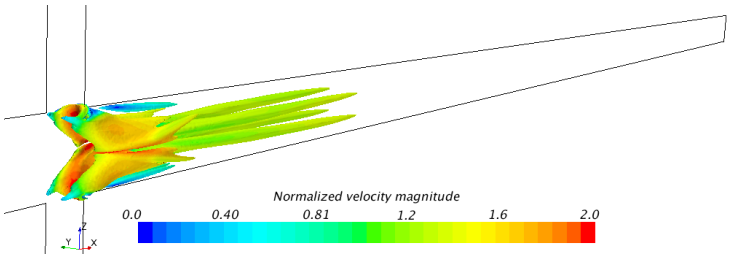


(a) xz-plane

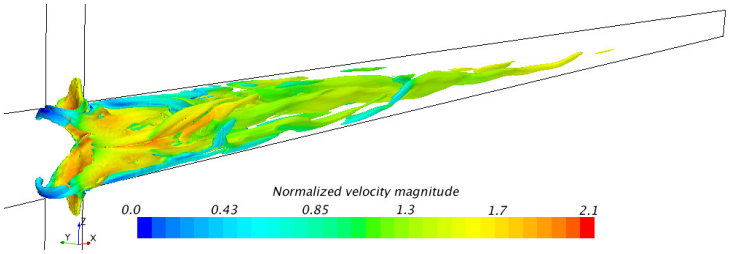
(b) xy-plane

(c) $0.5D$ (d) $1D$ (e) $2D$ (f) $5D$ (g) $10D$ (h) $15D$ (i) $20D$ (j) $25D$ (k)

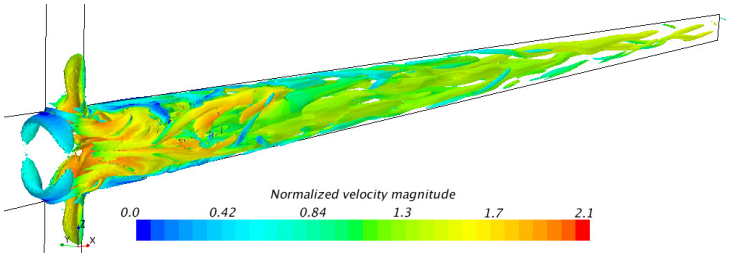
Figure 5: Time-averaged normalized velocity magnitude for 12 L/min in the (a) xz-plane, (b) xy-plane and (c-j) yz-plane at eight different diameters downstream of the mixing zone.



(a) 3 L/min



(b) 6 L/min



(c) 12 L/min

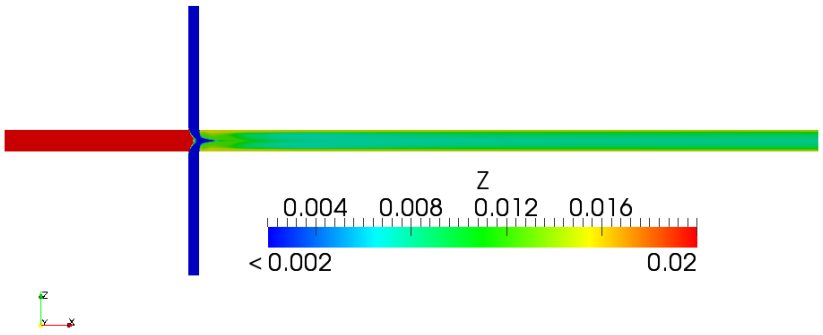
Figure 6: Iso-surfaces of the Q-criterion ($Q = +50000$) colored by normalized velocity magnitude.

tion dominated regions were more complex and random, and extended much further downstream. They eventually disappeared halfway downstream for the 6 L/min case, whereas the rotation dominated regions were sustained throughout the length of the domain for the 12 L/min case. This is further supported by the computed Reynolds numbers based on the flow rates in the main pipe, which also suggest that the flow will laminarize as long as the flow rate does not exceed 10 L/min.

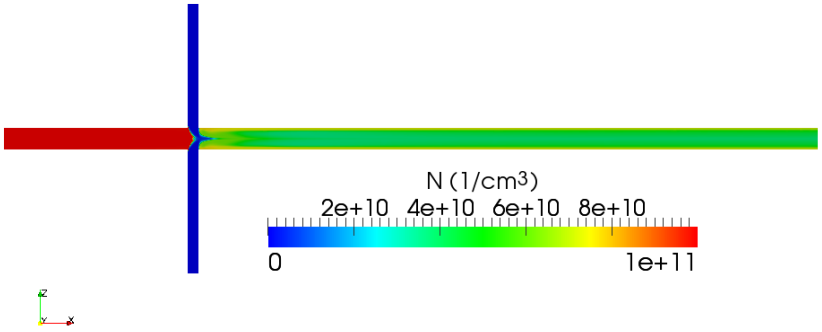
The dilution of the flow, using a double-tee junction with two collapsing jets, caused transition to turbulence in the shear layers created by the dilution jets, enhancing the mixing of the aerosol, and making the flow uniform in terms of aerosol concentration. Flow laminarization towards the outlet, representing the first aerosol sampling location in the VC24/48 exposure system, was present. Only in the highest 12 L/min flow rate case is the turbulent flow still sustained after the initial mixing region, until the very end of the computational domain. For more detailed flow-field analyses of the double-tee junction, please refer to the work by Kuczaj et al. (2016).

3.2. Coalescence simulations

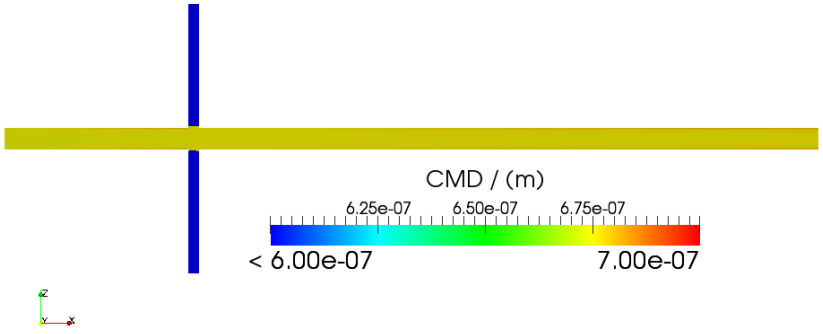
As already mentioned, the probability of coalescence influencing the aerosol size is increased with particle number density N and scales with γN^2, where γ is the coalescence rate coefficient that depends on the collision kernel (particle interactions). The effect of coalescence on the droplet size distribution is therefore presented for a high $N = 10^{11}$ 1/cm^3. The selected N is representative for the upper range of the droplet number density reported for cigarette smoke and aerosols generated by electronic cigarettes (see (Rostami, 2009)). The flow rate chosen for the study was 3 L/min. Instantaneous snapshots of Z, N and CMD from a developed flow condition are shown in Figure 7. The dilution resulted in a reduction of the liquid mass fraction Z by a factor of two after the double-tee junction (Figure 7a). Towards the outlet, only small fluctuations are visible in liquid mass fraction Z, indicating that the aerosol was almost uniformly mixed when it reached the outlet. A similar pattern was also observed for particle number density N in Figure 7b, where N was effectively and almost instantaneously diluted by the double-tee junction.



(a)



(b)



(c)

Figure 7: Influence of dilution and droplet coalescence for initial $N = 10^{11}$ $[1/cm^3]$ and $Z = 0.02$ shown by visualization of instantaneous snapshots of the liquid mass fraction Z, droplet number density N and CMD for a developed double-tee junction mixing simulations for 3 L/min.

The downstream diluted particle number density was also found to be close to uniform, which indicates that the mixing by the two opposing dilution jets was efficient. The aerosol size quantified by the value of count-median diameter CMD, computed from Z and N, remained constant in the main pipe, despite the observation that the aerosol was circumventing the two dilution jets through a reduced cross-section, as observed in Figure 3. This indicates that because of short aerosol residence time, there was no significant influence on the coalescence on the aerosol characteristics for the investigated case, which was already in the high end of the droplet number density ranges reported for cigarette smoke and aerosols generated by electronic cigarettes. This behavior indicates that coalescence can play important role directly during the exhaustion of the aerosol from the aerosol generator into the pump and consecutive entrance of it into the VC 24/48 (Figure 1).

4. Discussion

From the simulations, we observed that for the 3 L/min and the 6 L/min flow rate cases, the aerosol was efficiently mixed by local turbulent structures in a jet-mixing regime close to center of the double-tee junction. The flow thereafter quickly laminarized as expected from the computed Reynolds numbers. For the 12 L/min flow rate case, turbulent structures were shown to stretch throughout the domain, which did not lead to an abrupt laminarization of the flow. This was also visible in the presented visualization of the Q-criterion. According to the computed Reynolds numbers in the dilution pipes, the flow in the dilution inlets was also laminar below 2 L/min. Hence, operating below 4 L/min for a single dilution point without exceeding 10 L/min in total for all rows should guarantee that turbulent flow is avoided at the locations of the aerosol sampling trumpet pipes of the VC24/48 exposure system. The symmetry of the flow was fully maintained for the 3 L/min flow rate, whereas small asymmetric patterns were observed for the 6 L/min case. For the 12 L/min flow rate, the flow revealed a completely irregular pattern induced by the turbulent flow.

The introduction of an aerosol flow through the inlet of the main pipe showed that the aerosol is diluted efficiently by the two opposing dilution jets and accompanied turbulent mixing. This was clearly visible by the decreased liquid mass fraction and the close to uniform Z and N profiles close to the outlet of the domain. Only small non-uniformities remained in Z and N at the outlet, i.e., at the location of the first aerosol sampling trumpet

of the VC24/48 exposure system. Interestingly, the CMD remained constant in the main pipe, indicating that the coalescence time scales are longer than the considered flow residence time in the dilution unit and that even at such high droplet number concentrations the coalescence does not influence the aerosol droplet sizes in the VC24/48 exposure system under the considered simulation conditions.

5. Conclusions

We found that for all simulated flow rates, instantaneous and localized turbulent mixing is induced by the two opposing dilution jets. The flow generally laminarizes prior to the location of the first aerosol sampling trumpet of the VC24/48 exposure system. It was shown that the aerosol is uniformly mixed by the dilution jets and that both the liquid mass fraction and droplet number concentration are approximately uniform at the outlet. At 12 L/min the turbulent structures are more pronounced and sustainable throughout the entire domain. The results also showed that for the considered droplet number density and flow rates, the time scales of thermal coalescence are longer than the residence time of droplets in the dilution unit of the VC24/48. As a direct result, the thermal coalescence does not play a significant role and does not induce changes to the droplet size distribution. Localized effects of turbulent coalescence were not taken into account in this work and are a subject for future investigations. In summary, the design of the double-tee junction dilution unit of the VC24/48 guarantees efficient and localized mixing/dilution of the aerosol, while still delivering laminar flow towards deposition wells, when operated under high flow rate conditions. The symmetry of the opposing jets configuration supports the mixing of the flow inside of the main pipe and minimizes effects of potential high velocity jets directing the flow towards the walls, causing increased localized deposition. The extent of the mixing and potential modulation of the aerosol can be controlled by the user by applying different dilution flow rates.

Acknowledgments

The research described in this report was funded by Philip Morris Products S.A., Switzerland

Disclosure

A.K., M.N., J.H., and M.P. are employees of Philip Morris International. Philip Morris International is the sole source of funding and sponsor of this project. S.J. and E.K. are employees of NRG, which was contracted and paid by Philip Morris International to perform numerical studies. T.K. is the Managing Director of VITROCELL Systems GmbH, which supplies the VC24/48 system.

References

H. Hinds, Aerosol Technology: Properties, Behavior, and Measurement of Airborne Particles, 2nd ed., John Wiley & Sons Inc., New York, 1999.

C. Mathis, C. Poussin, D. Weisensee, S. Gebel, A. Hengstermann, A. Sewer, V. Belcastro, Y. Xiang, S. Ansari, S. Wagner, J. Hoeng, M. Peitsch, Human bronchial epithelial cells exposed in vitro to cigarette smoke at the air-liquid interface resemble bronchial epithelium from human smokers, Am J Physiol Lung Cell Mol Physiol 304 (2013) L489–503.

M.-J. W. A. Schiffelers, B. J. Blaauboer, C. F. M. Hendriksen, W. E. Bakker, Regulatory acceptance and use of 3R models: a multilevel perspective, ALTEX 29 (2012) 287–300.

European Parliament, Directive 2010/63/EU of the European Parliament and of the Council of 22 September 2010 on the protection of animals used for scientific purpose, Official J Eur Union L276 (2010) 33–79.

D. Thorne, J. Adamson, A review of in vitro cigarette smoke exposure systems, Experimental and Toxicologic Pathology 65 (2013) 1183–1193.

H.-R. Paur, F. Cassee, J. Teeguarden, H. Fissan, S. Diabate, M. Aufderheide, W. Kreyling, O. Hnninen, G. Kasper, B. Riediker, M. Rothen-Rutishauser, O. Schmid, In vitro cell exposure studies for the assessment of nanoparticle toxicity in the lung – a dialog between aerosol science and biology, Journal of Aerosol Science 42 (2011) 668–692.

A. Tippe, U. Heinzmann, C. Roth, Deposition of fine and ultrafine aerosol particles during exposure at the air/cell interface, Journal of Aerosol Science 33 (2002) 207–218.

A. Comouth, H. Saathoff, K.-H. Naumann, S. Muelhopt, H.-R. Paur, T. Leisner, Modelling and measurement of particle deposition for cell exposure at the air-liquid interface, Journal of Aerosol Science 63 (2013) 103–114.

A. R. Iskandar, F. Martin, M. Talikka, W. K. Schlage, R. Kostadinova, C. Mathis, J. Hoeng, M. C. Peitsch, Systems approaches evaluating the perturbation of xenobiotic metabolism in response to cigarette smoke exposure in nasal and bronchial tissues, Biomed Res Int 2013 (2014) 512086.

L. Neilson, C. Mankus, D. Thorne, G. Jackson, J. DeBay, C. Meredith, Development of an in vitro cytotoxicity model for aerosol exposure using 3D reconstructed human airway tissue; application for assessment of e-cigarette aerosol, Toxicology in Vitro 29 (2015) 1952–1962.

S. Majeed, S. Frentzel, S. Wagner, D. Kuehn, P. Leroy, P. A. Guy, A. Knorr, J. Hoeng, M. C. Peitsch, Characterization of the Vitrocell® 24/48 in vitro aerosol exposure system using mainstream cigarette smoke, Chemistry Central Journal 8 (2014).

J. Adamson, D. Thorne, G. Errington, W. Fields, X. Li, R. Payne, T. Krebs, A. Dalrymple, K. Fowler, D. Dillon, F. Xie, C. Meredith, An inter-machine comparison of tobacco smoke particle deposition in vitro from six independent smoke exposure systems, Toxicology in Vitro 7 (2014) 1320–1328.

J. Hoeng, R. Deehan, D. Pratt, F. Martin, A. Sewer, T. Thomson, D. Drubin, C. Waters, D. de Graaf, M. Peitsch, A network-based approach to quantifying the impact of biologically active substance, Drug Discov Today 17 (2012) 413–418.

S. Elghobashi, On predicting particle-laden turbulent flows, Journal of Applied Scientific Research 52 (1994) 309–329.

A. Guha, A unified Eulerian theory of turbulent deposition to smooth and rough surfaces, Journal of Aerosol Science 28 (1997) 1517–1537.

W. Hofmann, Modelling inhaled particle deposition in the human lung - a review, Journal of Aerosol Science 42 (2011) 693–724.

M. Nordlund, A. Kuczaj, Aerosol dosimetry modeling using computational fluid dynamics, in: J. Hoeng, M. Peitsch (Eds.), Computational Systems

Toxicology, Methods in Pharmacology and Toxicology, Springer, Humana Press, 2015.

S. Hangal, K. Willeke, Aspiration efficiency: unified model for all forward sampling angles, Environmental Science & Technology 24 (1990) 688–691.

A. Kuczaj, M. Nordlund, S. Jayaraju, E. Komen, Flow characterization in a double-tee junction dilution unit of exposure system, to be submitted (2016).

G. Pan, H. Meng, An experimental study of turbulent mixing in a tee mixer using PIV and PLIF, AIChE Journal 47 (2001) 2653–2665.

B. Asgharian, O. Price, J. Schroeter, J. Kimbell, M. Singal, A lung dosimetry model of vapor uptake and tissue disposition, Inhalation Toxicology 24 (2012) 182–193.

A. Rostami, Computational modeling of aerosol deposition in respiratory tract: A review, Inhalation Toxicology 21 (2009) 262–290.

C. Winkelmann, A. Kuczaj, M. Nordlund, B. Geurts, Simulation of aerosol formation due to rapid cooling of multispecies vapors, Submitted (2015).

K. Lee, H. Chen, Coagulation rate of polydisperse particles, Aerosol Science and Technology 3 (1984) 327–334.

S. Pope, Turbulent Flows, Cambridge Univ. Press, Cambridge, UK, 2000.

A. Tsinober, An informal conceptual introduction to turbulence, 2nd edn ed., Springer-Verlag, Dordrecht, 2009.

B. Geurts, Elements of direct and large-eddy simulation, R.T. Edwards, Inc., Philadelphia, 2003.

R. Deissler, Turbulent fluid motion, Taylor & Francis, Philadelphia, 1998.

A. Kuczaj, E. Komen, M. Loginov, Large Eddy Simulation study of turbulent mixing in a T-junction, Nuclear Engineering and Design 240 (2010) 2116–2122.

E. Komen, A. Shams, L. Camilo, B. Koren, Quasi-DNS capabilities of OpenFOAM for different mesh types, Computers and Fluids 96 (2014) 87–104.

A. Vreman, An eddy-viscosity subgrid-scale model for turbulent shear flow: Algebraic theory and applications 16 (2004) 3670–3681.

E. Frederix, M. Stanic, A. Kuczaj, M. Nordlund, B. Geurts, Extension of the compressible PISO algorithm to single-species aerosol formation and transport 74 (2015) 184–194.

R. Issa, B. Ahmadi-Befrui, K. Beshay, A. Gosman, Solution of the implicitly discretised reacting flow equations by operator-splitting, Journal of Computational Physics 93 (1991) 388–410.

J. C. R. Hunt, A. A. Wray, P. Moin, Eddies, Stream, and Convergence Zones in Turbulent Flows, Center For Turbulence Research Report CTR-S88 (1988).

Y. Dubief, F. Delcayre, On coherent-vortex identification in turbulence, Journal of Turbulence 1 (2000).